

Water Affects the Stereochemistry and Dioxygen Reactivity of Carboxylate-Rich Diiron(II) Models for the Diiron Centers in Dioxygen-Dependent Non-Heme Enzymes

Sungho Yoon and Stephen J. Lippard*

Contribution from the Department of Chemistry, Massachusetts Institute of Technology, Cambridge, Massachusetts 02139

Received February 28, 2005; E-mail: lippard@mit.edu

Abstract: Carboxylate-bridged high-spin diiron(II) complexes with distinctive electronic transitions were prepared by using 4-cyanopyridine (4-NCC₅H₄N) ligands to shift the charge-transfer bands to the visible region of the absorption spectrum. This property facilitated quantitation of water-dependent equilibria in the carboxylate-rich diiron(II) complex, [Fe₂(μ-O₂CAr^{Tol})₂(4-NCC₅H₄N)₂] (**1**), where ⁻O₂CAr^{Tol} is 2,6-di-(*p*-tolyl)benzoate. Addition of water to **1** reversibly shifts two of the bridging carboxylate ligands to chelating terminal coordination positions, converting the structure from a paddlewheel to a windmill geometry and generating [Fe₂(μ-O₂CAr^{Tol})₂(O₂CAr^{Tol})₂(4-NCC₅H₄N)₂(H₂O)₂] (**3**). This process is temperature dependent in solution, rendering the system thermochromic. Quantitative treatment of the temperature-dependent spectroscopic changes over the temperature range from 188 to 298 K in CH₂Cl₂ afforded thermodynamic parameters for the interconversion of **1** and **3**. Stopped flow kinetic studies revealed that water reacts with the diiron(II) center ca. 1000 times faster than dioxygen and that the water-containing diiron(II) complex reacts with dioxygen ca. 10 times faster than anhydrous analogue **1**. Addition of {H(OEt₂)₂}⁺{BAR'₄}⁻, where BAR'₄⁻ is tetrakis(3,5-di(trifluoromethyl)phenyl)borate, to **1** converts it to [Fe₂(μ-O₂CAr^{Tol})₃(4-NCC₅H₄N)₂](BAR'₄)⁻ (**5**), which was also structurally characterized. Mössbauer spectroscopic investigations of solid samples of **1**, **3**, and **5**, in conjunction with several literature values for high-spin iron(II) complexes in an oxygen-rich coordination environment, establish a correlation between isomer shift, coordination number, and N/O composition. The products of oxygenating **1** in CH₂Cl₂ were identified crystallographically to be [Fe₂(μ-OH)₂(μ-O₂CAr^{Tol})₂(O₂CAr^{Tol})₂(4-NCC₅H₄N)₂·2(HO₂CAr^{Tol})] (**6**) and [Fe₆(μ-O)₂(μ-OH)₄(μ-O₂CAr^{Tol})₆(4-NCC₅H₄N)₄Cl₂] (**7**).

Introduction

Carboxylate-bridged diiron units constitute a commonly occurring element in a growing number of dioxygen-dependent metalloenzymes.^{1,2} Important members of this class include the R2 subunit of Class I ribonucleotide reductases (RNR-R2),^{3–5} soluble methane monooxygenase (sMMO),^{6,7} fatty acid desaturase (Δ⁹D),^{8,9} and toluene monooxygenase (ToMO).¹⁰ Although these metalloproteins share a common structural motif, their diiron centers are tuned to achieve diverse functions. There are

subtle differences among the crystallographically characterized enzyme active sites, including the binding modes of the carboxylates and the existence of variable numbers of water molecules. These distinctions and the surrounding polypeptide matrix alter the chemical properties of the core to achieve the physiologically defined enzyme functions. Understanding how these shared carboxylate-bridged diiron(II) units work, how the variable surroundings differentiate their chemical properties, and the manner in which their dioxygen-activation mechanisms relate to one another represents a challenging and active area of research in bioinorganic chemistry.

Considerable effort has been expended to synthesize and study diiron complexes as analogues of the enzyme active sites in order to enrich our understanding of the chemistry of these systems at the molecular level.¹¹ A major goal is to reproduce the architecture of the enzyme active sites using carboxylate-based ligand frameworks and then to investigate the oxygenation of the resulting carboxylate-rich diiron(II) complexes. Two features that, until now, have best been appreciated mainly through direct studies of the biomolecules themselves⁶ and by

- (1) Holm, R. H.; Kennepohl, P.; Solomon, E. I. *Chem. Rev.* **1996**, *96*, 2239–2314.
- (2) Solomon, E. I.; Brunold, T. C.; Davis, M. I.; Kemsley, J. N.; Lee, S.-K.; Lehnert, N.; Neese, F.; Skulan, A. J.; Yang, Y.-S.; Zhou, J. *Chem. Rev.* **2000**, *100*, 235–349.
- (3) Stubbe, J.; van der Donk, W. A. *Chem. Rev.* **1998**, *98*, 705–762.
- (4) Logan, D. T.; Su, X.-D.; Åberg, A.; Regnström, K.; Hajdu, J.; Eklund, H.; Nordlund, P. *Structure* **1996**, *4*, 1053–1064.
- (5) Bollinger, J. M., Jr.; Edmondson, D. E.; Huynh, B. H.; Filley, J.; Norton, J. R.; Stubbe, J. *Science* **1991**, *253*, 292–298.
- (6) Merckx, M.; Kopp, D. A.; Sazinsky, M. H.; Blazyk, J. L.; Müller, J.; Lippard, S. J. *Angew. Chem., Int. Ed.* **2001**, *40*, 2782–2807.
- (7) Elango, N.; Radhakrishnan, R.; Froland, W. A.; Wallar, B. J.; Earhart, C. A.; Lipscomb, J. D.; Ohlendorf, D. H. *Protein Sci.* **1997**, *6*, 556–568.
- (8) Lindqvist, Y.; Huang, W.; Schneider, G.; Shanklin, J. *EMBO J.* **1996**, *15*, 4081–4092.
- (9) Broadwater, J. A.; Ai, J.; Loehr, T. M.; Sanders-Loehr, J. S.; Fox, B. G. *Biochemistry* **1998**, *37*, 14664–14671.
- (10) Sazinsky, M. H.; Bard, J.; Di Donato, A.; Lippard, S. J. *J. Biol. Chem.* **2004**, *279*, 30610, and refs. cited therein.

- (11) Du Bois, J.; Mizoguchi, T. J.; Lippard, S. J. *Coord. Chem. Rev.* **2000**, *200–202*, 443–485.

theoretical methods¹² are the effects of water molecules in the diiron coordination environment and the influence of the surrounding polypeptide matrix. The importance of certain amino acid residues in the surrounding polypeptide can be probed by selective mutagenesis.^{13,14} The effect of water on the oxygenation cycle has mainly been a focus of computational studies, however. In recently published DFT calculations the coordinated H₂O molecule, used as a hydrogen-bond donor, was considered to be a key component in forming reactive intermediate(s) upon oxygenation of the diiron(II) site.¹⁵ The participation of water in the oxygenation chemistry of the diiron protein core has also been invoked by ¹⁸O₂ studies in which the labeled oxygen atom is not fully incorporated into the products.¹⁶

Recently, we have begun to address the role that coordinated water might play in the oxygenation cycle of carboxylate-rich diiron sites in metalloenzymes by using small molecule synthetic mimics. The reaction between water and carboxylate-rich diiron(II) complexes has been qualitatively investigated and iron(II) complexes with varying numbers of water ligands isolated, revealing that the nature of the isolated carboxylate-bridged diiron(II) complexes is quite responsive to water present in the reaction mixture.^{17,18} Herein we report our efforts to treat the water-dependent equilibria quantitatively and to address the effects of water on the rate of oxygenation of the diiron(II) carboxylate complexes. These studies were facilitated by the introduction of 4-cyanopyridine (4-NCC₅H₄N) as a ligand, which shifts the metal-to-ligand charge-transfer bands of the starting diiron(II) compounds into the visible region of the spectrum. In addition, a correlation between isomer shifts in the Mössbauer spectra and coordination number for high-spin iron(II) carboxylate complexes was discovered through comparison of the new diiron(II) complexes with related ones in the literature.

Experimental Section

General Considerations. All reagents, including 4-NCC₅H₄N, were obtained from commercial suppliers and used as received unless otherwise noted. Dichloromethane, pentane, toluene, and THF were saturated with argon and purified by passage through activated Al₂O₃ columns under argon.¹⁹ Dioxygen (99.994%, BOC Gases) was dried by passing the gas stream through Drierite. The compounds [Fe₂(μ-O₂CAr^{Tol})₂(O₂CAr^{Tol})₂(THF)₂]²⁰ where ⁻O₂CAr^{Tol} = (p-tolyl)benzoate,^{21,22} [Fe₂(μ-O₂CAr^{4F-Ph})₂(CAr^{4F-Ph})₂(THF)₂]²⁰ where ⁻O₂CAr^{4F-Ph} is 2,6-di-(p-fluorophenyl)benzoate,^{21,22} and {H(OEt)₂}-{BAR'₄},²³ where BAR'₄ is tetrakis(3,5-di(trifluoromethyl)phenyl)borate, were prepared as described in the literature. Air-sensitive manipu-

lations were carried out under nitrogen in an MBraun glovebox. FT-IR spectra were recorded with a Thermo Nicolet Avatar 360 spectrometer. UV-vis spectra were obtained on a Hewlett-Packard 8453 diode array spectrophotometer. During variable temperature UV-vis studies, the temperature was controlled with an Oxford ITC 601 cryostat.

[Fe₂(μ-O₂CAr^{Tol})₂(4-NCC₅H₄N)₂] (1). To a light yellow solution of [Fe₂(μ-O₂CAr^{Tol})₂(O₂CAr^{Tol})₂(THF)₂] (1.85 g, 1.26 mmol) in CH₂Cl₂ (100 mL) was added solid 4-NCC₅H₄N (263 mg, 2.53 mmol), and the dark red pink solution was stirred for 20 min. The solution was filtered through Celite, and pentane was layered on top. Dichroic red pink blocks of **1** (1.44 g, 75%) formed overnight. The best crystals for X-ray diffraction study were obtained by recrystallization from THF/pentane. FT-IR (KBr, cm⁻¹) 3050 (w), 3021 (w), 2918 (w), 2862 (w), 2236 (w, ν_{C≡N}), 1609 (s), 1551 (w), 1513 (w), 1493 (w), 1440 (m), 1404 (m), 1384 (s), 1303 (w), 1215 (w), 1188 (w), 1109 (w), 1065 (w), 843 (w), 814 (s), 789 (m), 762 (w), 727 (w), 706 (m), 580 (w), 558 (w), 526 (m). Anal. Calcd for **1**·0.5(CH₂Cl₂), isolated from methylene chloride, C₁₀₃H₉₃Fe₂N₄O₈Cl: C, 73.93; H, 4.95; N, 3.57. Found: C, 74.44; H, 5.10; N, 3.40.

[Fe₂(μ-O₂CAr^{4F-Ph})₂(4-NCC₅H₄N)₂] (2). To a rapidly stirred solution of [Fe₂(μ-O₂CAr^{4F-Ph})₂(O₂CAr^{4F-Ph})₂(THF)₂] (762 mg, 51.0 mmol) in CH₂Cl₂ (50 mL) was added solid 4-NCC₅H₄N (106 mg, 102 mmol), yielding a red solution. A red precipitate of **2** (512 mg, 65%) formed immediately and was isolated by filtration and washed with pentane. The solid (20.3 mg) was dissolved in CH₂Cl₂ (10 mL), and exposure of the solution to pentane vapor diffusion yielded dichroic yellow-red blocks, suitable for X-ray crystallography. FT-IR (KBr, cm⁻¹) 3056 (w), 2239 (w, ν_{C≡N}), 1610 (s), 1569 (w), 1551 (w), 1509 (s), 1452 (w), 1404 (m), 1382 (s), 1299 (w), 1220 (s), 1159 (m), 1095 (w), 844 (m), 832 (m), 818 (m), 793 (w), 773 (w), 727 (w), 706 (w), 582 (w), 556 (m), 532 (w). Anal. Calcd for C₈₈H₅₂F₈Fe₂N₄O₈: C, 67.88; H, 3.37; N, 3.60. Found: C, 67.55; H, 3.45; N, 3.72.

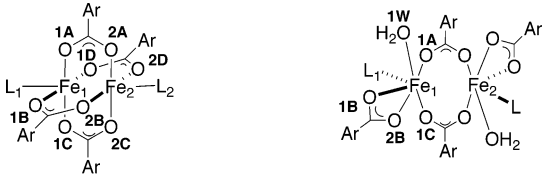
[Fe₂(μ-O₂CAr^{Tol})₂(O₂CAr^{Tol})₂(4-NCC₅H₄N)₂(OH₂)₂] (3). To a stirred yellow solution of [Fe₂(μ-O₂CAr^{Tol})₄(4-NCC₅H₄N)₂] (49.5 mg, 29.8 μmol) in THF (1 mL) was added slowly H₂O (7 μL) under nitrogen. Dichroic yellow-red needle crystals of **3** (20.3 mg, 44%), suitable for X-ray crystallography, were obtained by vapor diffusion of pentanes into the solution. FT-IR (KBr, cm⁻¹) 3653 (w), 3423 (w, br), 2918 (w), 2235 (w, ν_{C≡N}), 1609 (s), 1515 (s), 1452 (s), 1411 (m), 1381 (s), 1217 (w), 1190 (w), 1109 (w), 860 (w), 846 (w), 818 (s), 797 (m), 790 (m), 781 (m), 766 (w), 734 (w), 713 (w), 586 (w), 559 (m), 540 (w), 521 (w), 454 (w). Anal. Calcd for C₉₆H₈₀Fe₂N₄O₁₀: C, 73.85; H, 5.16; N, 3.59. Found: C, 73.85; H, 5.48; N, 3.81.

[Fe₂(μ-O₂CAr^{4F-Ph})₂(O₂CAr^{4F-Ph})₂(4-NCC₅H₄N)₂(OH₂)₂] (4). Compound **4** was synthesized as described for **3** and identified by X-ray crystallography (yield 58%). FT-IR (KBr, cm⁻¹) 3655 (w), 3420 (w, br), 3054 (w), 2244 (w, ν_{C≡N}), 1604 (s), 1510 (s), 1451 (s), 1409 (m), 1380 (s), 1301 (w), 1224 (s), 1160 (m), 1093 (w), 1011 (w), 852 (m), 833 (s), 814 (s), 807 (s), 789 (m), 773 (m), 733 (w), 712 (m), 701 (w), 556 (m), 527 (m), 464 (w). Anal. Calcd for C₈₈H₅₆F₈Fe₂N₄O₁₀: C, 65.04; H, 3.47; N, 3.45. Found: C, 65.55; H, 3.57; N, 3.70.

[Fe₂(μ-O₂CAr^{Tol})₃(4-NCC₅H₄N)₂][BAR'₄] (5). To a stirred red-pink solution of [Fe₂(μ-O₂CAr^{Tol})₄(4-NCC₅H₄N)₂] (14.5 mg, 8.7 μmol) in CH₂Cl₂ (3 mL) was added 1 equiv of {H(OEt)₂}{BAR'₄}, yielding a yellow solution under anaerobic conditions. The solution was filtered through Celite, and pentane was diffused into it. Yellow-red blocks of **5** (12.3 mg, 68%), suitable for X-ray crystallography, formed overnight. FT-IR (KBr, cm⁻¹) 3051 (w), 2920 (w), 2237 (ν_{C≡N}), 1614 (m), 1585 (s), 1514 (s), 1493 (s), 1436 (w), 1405 (m), 1385 (m), 1271 (m), 1219 (w), 1030 (w), 832 (s), 807 (s), 791 (m), 636 (w), 586 (m), 560 (w), 528 (w). Anal. Calcd for **5**·0.5(CH₂Cl₂) or C_{107.5}H₇₂BClF₂₄Fe₂N₄O₆: C, 60.63; H, 3.41; N, 2.63. Found: C, 60.74; H, 3.56; N, 3.02.

[Fe₂(μ-OH)₂(μ-O₂CAr^{Tol})₂(O₂CAr^{Tol})₂(4-NCC₅H₄N)₂]·2(HO₂-CAr^{Tol}) (6) and [Fe₆(μ-O)₂(μ-OH)₄(μ-O₂CAr^{Tol})₆(4-NCC₅H₄N)₄(Cl)₂] (7). A pink-red solution of **1** (15 mg, 0.017 mmol) in CH₂Cl₂ (10 mL) was saturated with dry dioxygen by bubbling over a period of 10 min,

- (12) Gherman, B. F.; Baik, M.-H.; Lippard, S. J.; Friesner, R. A. *J. Am. Chem. Soc.* **2004**, *126*, 2978–2990.
- (13) Skulan, A. J.; Brunold, T. C.; Baldwin, J.; Saleh, L.; Bollinger, J. M., Jr.; Solomon, E. I. *J. Am. Chem. Soc.* **2004**, *126*, 8842–8855.
- (14) Fox, B. G.; Lyle, K. S.; Rogge, C. E. *Acc. Chem. Res.* **2004**, *37*, 421–429.
- (15) Baik, M.-H.; Newcomb, M.; Friesner, R. A.; Lippard, S. J. *Chem. Rev.* **2003**, *103*, 2385–2419.
- (16) Moe, L. A.; Hu, Z.; Deng, D.; Austin, R. N.; Groves, J. T.; Fox, B. G. *Biochemistry* **2004**, *43*, 15688–15701.
- (17) Yoon, S.; Kelly, A. E.; Lippard, S. J. *Polyhedron* **2004**, *23*, 2805–2812.
- (18) Yoon, S.; Lippard, S. J. *J. Am. Chem. Soc.* **2004**, *126*, 16692–16693.
- (19) Pangborn, A. B.; Giardello, M. A.; Grubbs, R. H.; Rosen, R. K.; Timmers, F. J. *Organometallics* **1996**, *15*, 1518–1520.
- (20) Lee, D.; Lippard, S. J. *Inorg. Chem.* **2002**, *41*, 2704–2719.
- (21) Du, C.-J. F.; Hart, H.; Daniel Ng, K.-K. *J. Org. Chem.* **1986**, *51*, 3162–3165.
- (22) Chen, C.-T.; Siegel, J. S. *J. Am. Chem. Soc.* **1994**, *116*, 5959–5960.
- (23) Brookhart, M.; Grant, B.; Volpe, A. F., Jr. *Organometallics* **1992**, *11*, 3920–3922.

Table 1. Selected Bond Lengths (Å) for **1–4**^a


	1 and 2		3 and 4	
	1	2	3	4
Fe1...Fe2	2.7754(9)	2.7415(16)	4.4658(13)	4.4019(10)
Fe1–O1A	2.032(3)	2.036(5)	2.0285(13)	2.0485(15)
Fe1–O1B	2.133(3)	2.120(5)	2.1475(13)	2.1565(15)
Fe1–O2B			2.3278(14)	2.3352(15)
Fe1–O1C	2.016(3)	2.040(5)	2.0871(13)	2.0714(14)
Fe1–O1D	2.132(3)	2.112(5)		
Fe1–L1 ^b	2.091(4)	2.086(7)	2.1505(16)	2.1412(18)
Fe1–O1W			2.1686(15)	2.1552(18)
Fe2–O2A	2.131(3)	2.057(5)		
Fe2–O2B	2.010(3)	2.082(5)		
Fe2–O2C	2.145(3)	2.064(5)		
Fe2–O2D	2.004(3)	2.070(5)		
Fe2–L2 ^b	2.100(4)	2.097(7)		

^a Numbers in parentheses are estimated standard deviations in the last significant figures. ^b L indicates the aromatic ring nitrogen atom in 4-cyanopyridine. Atoms are labeled as indicated in Figures 1 and 2.

resulting in a yellow-green solution. The solution was filtered through Celite, and pentane was diffused into it. Light green blocks of **6** and yellow-brown blocks of **7** were obtained after several days. Although the structures of **6** and **7** could be determined by X-ray crystallography, bulk samples could not be obtained.

X-ray Crystallographic Studies. Single crystals were mounted at room temperature on the tips of quartz fibers, coated with Paratone-N oil, and cooled under a stream of cold nitrogen. Intensity data were collected on a Bruker (formerly Siemens) APEX CCD diffractometer running the SMART software package, with Mo K α radiation ($\lambda = 0.71073$ Å). Data collection and reduction protocols are described in detail elsewhere.²⁴ The structures were solved by both direct and Patterson methods and refined on F^2 by using the SHELXTL software package.²⁵ Empirical absorption corrections were applied with SADABS,²⁶ part of the SHELXTL program package, and the structures were checked for higher symmetry by the program PLATON.²⁷ All non-hydrogen atoms were refined anisotropically. In general, hydrogen atoms were assigned idealized positions and given thermal parameters equivalent to 1.2 (all other hydrogen atoms) times the thermal parameter of the atom to which they were attached. Hydrogen atoms of the bridging hydroxides and water molecules were located on difference electron density maps. In the structure of **1**, four THF molecules were assigned in the lattice and refined isotropically. The structure of **2** contains four CH₂Cl₂ molecules in the lattice. In the structure of **5**, one BAR₄[−] anion was assigned to two positions, each with a half occupancy factor and severe disorder. Four CH₂Cl₂ molecules were found in the lattice of compound **6**. There were six CH₂Cl₂ molecules in the lattice of compound **7**. Data collection and experimental details for the complexes are summarized in Table S1 (Supporting Information) and relevant interatomic bond lengths and angles for **1–4** are listed in Tables S2 and S3. Selected geometric details for complexes **1–4** are reported in Table 1.

⁵⁷Fe Mössbauer Spectroscopy. Zero-field Mössbauer spectra were recorded on an MS1 spectrometer (WEB Research Co.) with a ⁵⁷Co source in a Rh matrix maintained at room temperature in the Massachusetts Institute of Technology Department of Chemistry Instrument Facility (MIT DCIF). Solid samples were prepared by suspending ca. 30 mg of the powdered solids in Apeizon N grease and packing the mixture into a nylon sample holder. Data were collected at 4.2 K, and the isomer shift (δ) values are reported with respect to natural iron foil that was used for velocity calibration at room temperature. The spectra were fit to Lorentzian lines by using the WMOSS plot and fit program.²⁸

Resonance Raman Spectroscopy. Resonance Raman spectra were obtained by using an Ar⁺ ion laser with excitation provided at 514 nm. A monochromator (1200 grooves/nm grating) with an entrance slit of 10 μ m and a TE-CCD-1100-PB-VISAR detector cooled to 243 K with a circulating water bath was employed in a standard back-scattering configuration. Data were collected at 296 K in dichloromethane using an NMR tube. Each sample concentration was 6 mM. Measurements were made on more than one freshly prepared sample and in triplicate to ensure the authenticity of the results. The dichloromethane bands at 1156, 897, 704, and 286 cm^{−1} were used as an internal calibration standard. Data were processed using WinSpec 3.2.1 (Princeton Instruments, Inc.) and were further manipulated by Kaleidagraph.

Stopped-Flow Kinetics Experiments. All ambient-pressure kinetics experiments were carried out by using a Canterbury stopped-flow SF-40 and MG-6000 rapid diode array system (Hi-Tech Scientific), fitted with stainless steel flow lines and an argon-purged anaerobic attachment. Teflon-lined stainless steel flow lines, adopted in the previous generation of stopped-flow instruments, retain air and water, causing premature oxidation or aquation of air-sensitive solutions. The instrument was therefore rebuilt to avoid these problems. Solutions of **1** in CH₂Cl₂ (ca. 0.385 mM) were prepared in a glovebox under a nitrogen atmosphere and stored in a gastight syringe prior to loading into the stopped-flow apparatus. A saturated solution of dioxygen was prepared by bubbling the gas through CH₂Cl₂ for 20 min in a round-bottomed flask closed with a septum and maintained at 293 K. The saturated CH₂Cl₂ solution of dioxygen containing 2 mM water was prepared by bubbling the dioxygen gas into a solution of that composition.

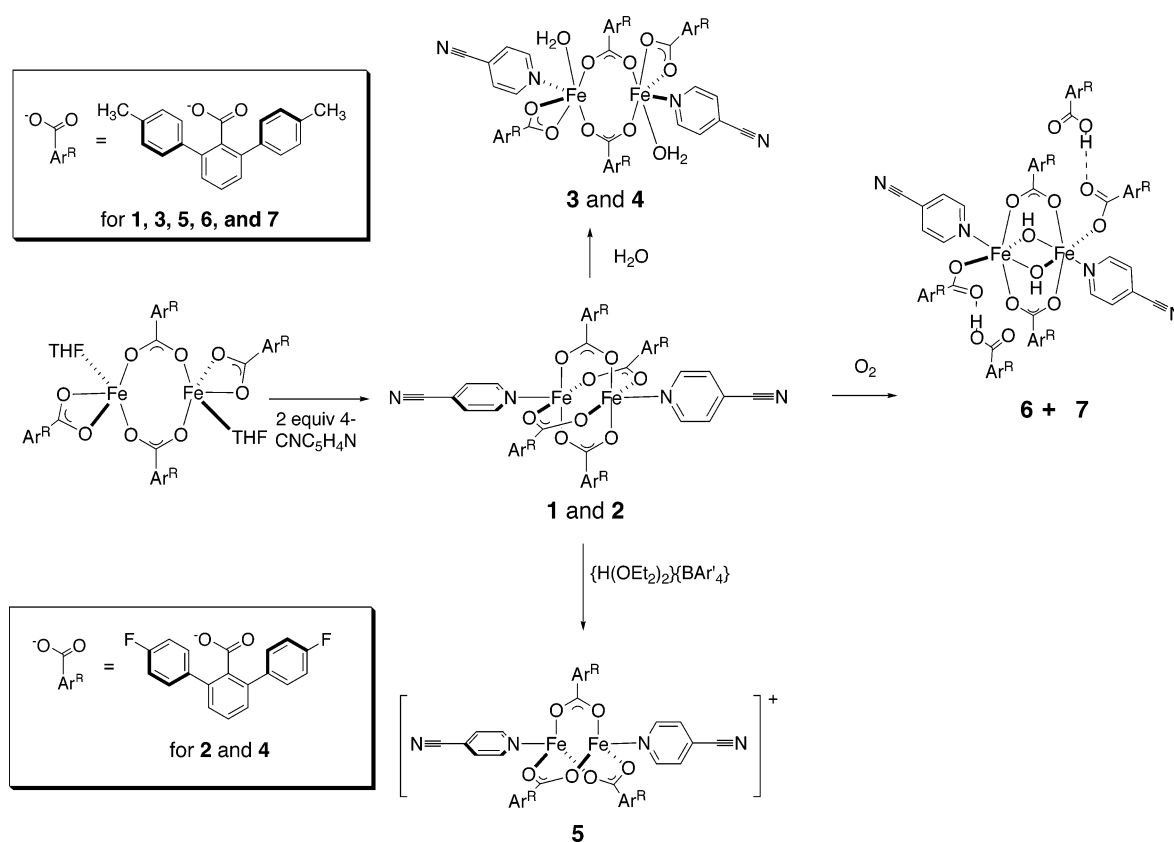
Results and Discussion

In contrast to the relatively rich optical absorption spectra afforded by low-spin iron(II) complexes, high-spin iron(II) analogues with carboxylate-rich coordination environments are typically colorless, making it difficult to apply standard UV–vis spectroscopic methods to follow their chemistry. For example, the charge-transfer band in the visible region of the spectrum are well documented for low-spin iron(II) complexes having pyridine ligands.^{29,30} On the other hand, most high-spin iron(II) complexes are colorless or at best light yellow.^{20,31–36} In our previous studies, the detection of water-dependent interconversions in carboxylate-rich diiron(II) complexes was achieved by using solid-state methods, chiefly X-ray crystallography.^{17,18} The inability to monitor these reactions in fluid solution by spectroscopy prohibited their definitive assignment as equilibrium phenomena. To treat the water-dependent reactions in a quantitative manner, assign equilibrium states, and address the effects of water on the oxygenation of high-spin diiron(II) complexes, an optical probe was highly desired. Just such a probe was discovered with the introduction of 4-cyanopyridine as a ligand.

- (24) Kuzelka, J.; Mukhopadhyay, S.; Spingler, B.; Lippard, S. J. *Inorg. Chem.* **2004**, *43*, 1751–1761.
 (25) Sheldrick, G. M. *Program Library for Structure Solution and Molecular Graphics*; Version 6.2, Bruker AXS: Madison, WI, 2000.
 (26) Sheldrick, G. M. *SADABS: Area-Detector Absorption Correction*; University of Göttingen: Göttingen, Germany, 2001.
 (27) Spek, A. L. *PLATON, A Multipurpose Crystallographic Tool*; Utrecht University: Utrecht, The Netherlands, 2000.

- (28) Kent, T. A. *WMOSS. Mössbauer Spectral Analysis Software*; Version 2.5, Minneapolis, MN, 1998.

Scheme 1



Synthesis and Structural Characterization of Diiron(II) Complexes $[\text{Fe}_2(\mu\text{-O}_2\text{CAR}^{\text{Totol}})_4(4\text{-NCC}_5\text{H}_4\text{N})_2]$ (**1**) and $[\text{Fe}_2(\mu\text{-O}_2\text{CAR}^{4\text{F-Ph}})_4(4\text{-NCC}_5\text{H}_4\text{N})_2]$ (**2**). A clue for how to access high-spin diiron(II) carboxylate complexes with visible absorption bands came from the electronic spectrum of the $[\text{Fe}_2(\mu\text{-O}_2\text{CAR}^{\text{Totol}})_4(4\text{-}^t\text{BuC}_5\text{H}_4\text{N})_2]$,^{20,37} which has a shoulder at 370 nm with $\epsilon = 1400 \text{ cm}^{-1} \text{ M}^{-1}$, thought to be a charge-transfer transition from Fe(II) to a π^* orbital of the pyridine ligand (MLCT). If this assignment is correct, we reasoned that, by lowering the energy of the acceptor orbital, it should be possible to narrow the energy gap between the states involved in this transition. This hypothesis was tested by synthesizing 4-NCC₅H₄N analogues of $[\text{Fe}_2(\mu\text{-O}_2\text{CAR}^{\text{Totol}})_4(4\text{-}^t\text{BuC}_5\text{H}_4\text{N})_2]$, anticipating a red shift of the electronic transition. Upon addition of 2 equiv of 4-NCC₅H₄N to a light yellow solution of $[\text{Fe}_2(\mu\text{-O}_2\text{CAR}^{\text{Totol}})_2(\text{O}_2\text{CAR}^{\text{Totol}})_2(\text{THF})_2]$ in CH_2Cl_2 , the color instantaneously turned to intense red-pink, affording the desired diiron(II) complex $[\text{Fe}_2(\mu\text{-O}_2\text{CAR}^{\text{Totol}})_4(4\text{-NCC}_5\text{H}_4\text{N})_2]$ (**1**) (Scheme 1). When isolated from solution, however, the crystals developed fissures, probably due to loss of solvent molecule(s) in the lattice. Figures 1 and

S1 display the structure and Tables 1 and S2 list selected interatomic distances and angles. Two crystallographically inequivalent square-pyramidal iron(II) centers, separated by 2.7754(9) Å, are linked by four bridging carboxylate ligands. The 4-NCC₅H₄N ligands coordinate to the iron(II) sites in axial positions through pockets that are generated by the four bulky carboxylate ligands. Most of geometric features of **1** are the same as in previously characterized paddle-wheel complexes $[\text{Fe}_2(\mu\text{-O}_2\text{CAR}^{\text{Totol}})_4(4\text{-}^t\text{BuC}_5\text{H}_4\text{N})_2]$ ³⁷ and $[\text{Fe}_2(\mu\text{-O}_2\text{CAR}^{\text{Totol}})_4(\text{BA}^{p\text{-OMe}})_2]$,³⁸ where $\text{BA}^{p\text{-OMe}}$ is 4-methoxybenzylamine. A powdered sample of **1** is stable in the solid state in air for over 2 months, judging by the maintenance of its distinctive color.

Treatment of a light yellow CH_2Cl_2 solution of $[\text{Fe}_2(\mu\text{-O}_2\text{CAR}^{4\text{F-Ph}})_2(\text{O}_2\text{CAR}^{4\text{F-Ph}})_2(\text{THF})_2]$ with 2 equiv of 4-NCC₅H₄N afforded the red diiron(II) complex $[\text{Fe}_2(\mu\text{-O}_2\text{CAR}^{4\text{F-Ph}})_4(4\text{-NCC}_5\text{H}_4\text{N})_2]$ (**2**) (Scheme 1), which is the structural analogue of **1** (Figure S2). Selected interatomic distances and angles are listed in Tables 1 and S2. Since **2** is not very soluble in most solvents, further studies were performed mainly with compound **1**.

Syntheses and Structural Characterization of Water-Containing Diiron(II) Complexes $[\text{Fe}_2(\mu\text{-O}_2\text{CAR}^{\text{Totol}})_2(\text{O}_2\text{CAR}^{\text{Totol}})_2(4\text{-NCC}_5\text{H}_4\text{N})_2(\text{OH}_2)_2]$ (**3**) and $[\text{Fe}_2(\mu\text{-O}_2\text{CAR}^{4\text{F-Ph}})_2(\text{O}_2\text{CAR}^{4\text{F-Ph}})_2(4\text{-NCC}_5\text{H}_4\text{N})_2(\text{OH}_2)_2]$ (**4**). Addition of **1** to a CH_2Cl_2 or THF solution containing a measured amount of water resulted in an instantaneous color change from red-pink to light yellow-red. Out of these solutions crystallized compound **3** following vapor diffusion of pentane into it. The structure of **3** is displayed in Figures 2 and S3, with interatomic distances

- (29) Monat, J. E.; McCusker, J. K. *J. Am. Chem. Soc.* **2000**, *122*, 4092–4097.
 (30) Roelfes, G.; Vrajmasu, V.; Chen, K.; Ho, R. Y. N.; Rohde, J.-U.; Zondervan, C.; la Crois, R. M.; Schudde, E. P.; Lutz, M.; Spek, A. L.; Hage, R.; Feringa, B. L.; Münck, E.; Que, L., Jr. *Inorg. Chem.* **2003**, *42*, 2639–2653.
 (31) Lee, D.; Lippard, S. J. *Inorg. Chim. Acta* **2002**, *341*, 1–11.
 (32) Hagadorn, J. R.; Que, L., Jr.; Tolman, W. B. *J. Am. Chem. Soc.* **1998**, *120*, 13531–13532.
 (33) Lee, D.; DuBois, J. L.; Pierce, B.; Hedman, B.; Hodgson, K. O.; Hendrich, M. P.; Lippard, S. J. *Inorg. Chem.* **2002**, *41*, 3172–3182.
 (34) Lee, D.; Hung, P.-L.; Spangler, B.; Lippard, S. J. *Inorg. Chem.* **2002**, *41*, 521–531.
 (35) Lee, D.; Lippard, S. J. *Inorg. Chem.* **2002**, *41*, 827–837.
 (36) Lee, D.; Pierce, B.; Krebs, C.; Hendrich, M. P.; Huynh, B. H.; Lippard, S. J. *J. Am. Chem. Soc.* **2002**, *124*, 3993–4007.
 (37) Lee, D.; Du Bois, J.; Petasis, D.; Hendrich, M. P.; Krebs, C.; Huynh, B. H.; Lippard, S. J. *J. Am. Chem. Soc.* **1999**, *121*, 9893–9894.

(38) Yoon, S.; Lippard, S. J. *Inorg. Chem.* **2003**, *42*, 8606–8608.

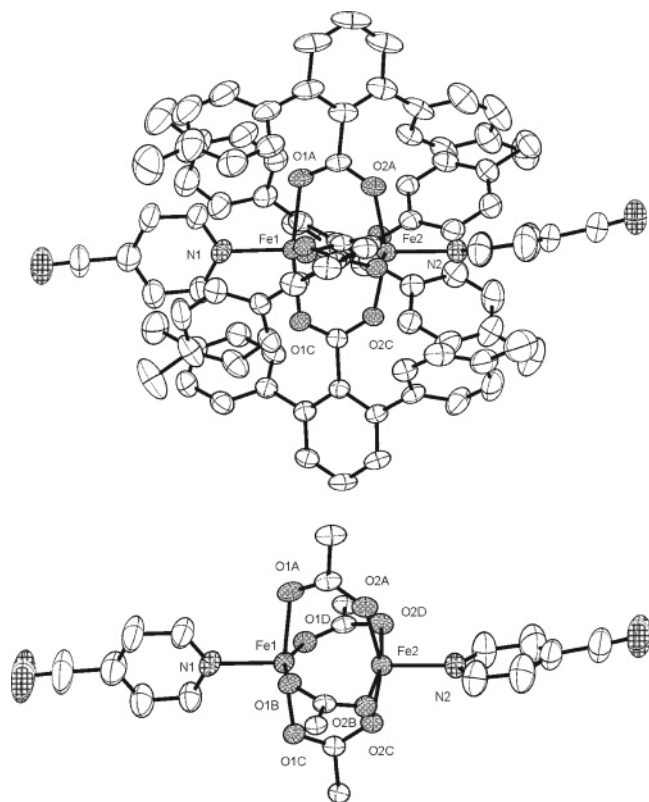


Figure 1. Top: ORTEP diagram of $[\text{Fe}_2(\mu\text{-O}_2\text{CAr}^{\text{Tol}})_4(4\text{-NCC}_5\text{H}_4\text{N})_2]$ (1) showing 50% probability thermal ellipsoids for all non-hydrogen atoms. Bottom: Structure with the aromatic rings of $\text{Ar}^{\text{Tol}}\text{CO}_2^-$ ligands omitted for clarity.

and angles listed in Tables 1 and S3. Two distorted octahedral iron(II) centers are bridged by two carboxylate ligands with an $\text{Fe}\cdots\text{Fe}$ separation of 4.4658(13) Å. This value is 1.69 Å longer than the $\text{Fe}\cdots\text{Fe}$ separation of 2.7754(9) Å in **1** and arises from water-induced shifting of two carboxylate ligands from a bridging to a terminal chelating mode. The reaction typifies how the binding of water in carboxylate-bridged diiron(II) complexes can induce a dramatic structural change. The nonbridging coordination sites are occupied by 4-NCC₅H₄N, water, and the bidentate terminal carboxylate ligands. The assignment of water as the ligand rather than hydroxide is based on the $\text{Fe}\text{--}\text{O}(\text{aqua})$ distance, 2.1686(15) Å, the location and refinement of the associated hydrogen atoms in the X-ray structure determination ($\text{O}\text{--}\text{H}$, 0.71 and 0.86 Å), and charge considerations. Inter- and intramolecular hydrogen bonding interactions between the metal-bound water molecules and the carboxylate ligand are characterized by short $\text{O}\cdots\text{H}\cdots\text{O}$ distances, ranging from 2.731 Å to 2.755 Å (Figure 2, bottom). The intermolecular hydrogen bonds may contribute to the observed hardness of the crystals. When **3** is dissolved in anhydrous CH_2Cl_2 , a red-pink color is obtained instead of red-yellow, indicating that the coordinated water ligands observed in the solid state are readily displaced from the first coordination sphere. Compound **4** is essentially isostructural with **3** (Figure S4 and Table S3).

Synthesis and Characterization of $[\text{Fe}_2(\mu\text{-O}_2\text{CAr}^{\text{Tol}})_3(4\text{-NCC}_5\text{H}_4\text{N})_2](\text{BAR}_4^-)$ (5) Upon Reaction of Compound 1 with H^+ . When compound **1** was titrated with a CH_2Cl_2 solution of $[\text{H}(\text{OEt})_2]\{\text{BAR}_4^-\}$,²³ the intense red-pink color disappeared following addition of ca. 1.2 equiv of the acid, generating a yellow solution. Although the structure of **5** could be determined

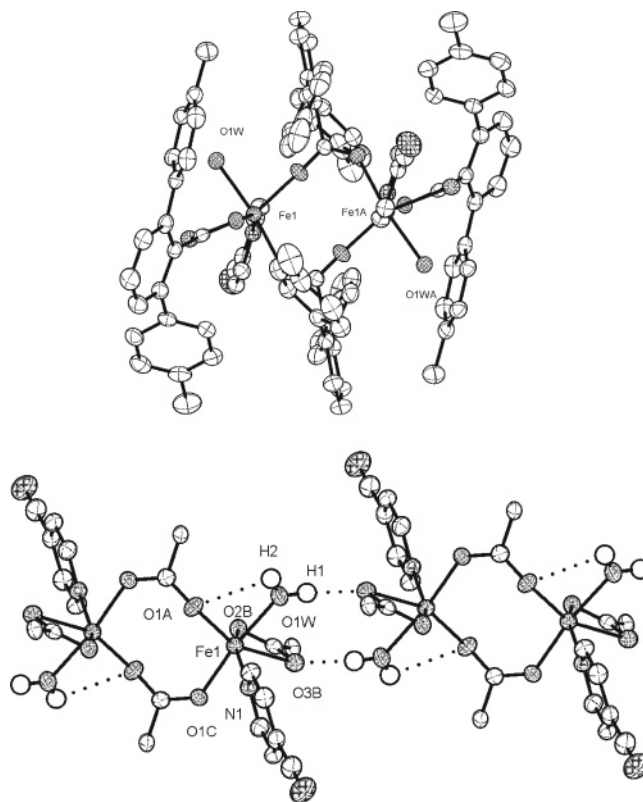


Figure 2. Top: ORTEP diagram of $[\text{Fe}_2(\mu\text{-O}_2\text{CAr}^{\text{Tol}})_2(\text{O}_2\text{CAr}^{\text{Tol}})_2(4\text{-NCC}_5\text{H}_4\text{N})_2(\text{OH}_2)_2]$ (3) showing 50% probability thermal ellipsoids for all non-hydrogen atoms. Bottom: Structure with the aromatic rings of $\text{Ar}^{\text{Tol}}\text{CO}_2^-$ ligands omitted for clarity and depicting H-bonding interactions (dotted lines).

by X-ray crystallography, the large unit cell volume and severe disorder in the BAR_4^- counterion prohibited satisfactory refinement. Drawings of **5** are depicted in Figure S5. The two pseudo-tetrahedral iron(II) sites with NO_3 coordination geometries are bridged by three carboxylates at an $\text{Fe}\cdots\text{Fe}$ distance of 3.11 Å. Two 4-NCC₅H₄N ligands coordinate to the iron(II) sites through the pockets generated by the three bulky carboxylate ligands.

Mössbauer Spectroscopy. Correlation of Isomer Shift with Core Composition. Zero-field Mössbauer spectra of solid samples of **1**, **2**, **3**, and **5** were recorded at 4.2 K in the absence of an external field. These spectra are displayed in Figures S6 and S7 and Mössbauer parameters are listed in Table 2, which also includes results for related carboxylate-rich iron(II) complexes and enzymes of interest. The Mössbauer spectra of both **1** and **2** exhibit slightly asymmetric quadrupole doublets, probably reflecting the inequivalence of the two iron atoms in the crystal lattice. By contrast, the iron centers of compound **3** are crystallographically equivalent, resulting in spectra that are symmetric. The isomer shifts of these compounds compare well with those of other high-spin iron(II) complexes having oxygen-rich coordination environments, indicating that compounds **1**–**3** and **5** have high spin $S = 2$ ground states.³⁹

One obvious trend in the data of Table 2 is that iron(II) sites with coordination number 4 tend to have lower isomer shifts (1.0–1.1 mm s^{-1}) compared to coordinatively saturated iron(II) centers ($\sim 1.3 \text{ mm s}^{-1}$). A possible explanation for this trend is

(39) Tshuva, E. Y.; Lippard, S. J. *Chem. Rev.* **2004**, *104*, 987–1012.

Table 2. Zero-Field Mössbauer Parameters at 4.2 K for **1–3**, **5**, Carboxylate-Rich Iron(II) Complexes, and Related Enzymes

		coordination geometry	δ (mm s ⁻¹)	ΔE_Q (mm s ⁻¹)	ref
[Fe(O ₂ CAr ^{4F-Ph}) ₂ (Hdmpz) ₂]		<i>Td</i> , ^a N ₂ O ₂	1.04(2)	3.19(2)	<i>i</i>
5		<i>Td</i> , NO ₃	1.04(2)	2.85(2)	<i>h</i>
[Fe(O ₂ CAr ^{Tol}) ₂ (1-BuIm) ₂]		<i>Td</i> , N ₂ O ₂	1.08(2)	2.46(2)	31
[Fe ₂ (μ-O ₂ CAr ^{Tol}) ₃ (O ₂ CAr ^{Tol})(2,6-lutidine) ₂]	site 1	<i>Td</i> , NO ₃	1.05(2)	2.18(2)	31
	site 2	<i>Tbp</i> , ^b O ₅	1.23(2)	2.80(2)	
[Fe(O ₂ CAr ^{Tol}) ₂ (BPTA) ₂]		<i>Tbp</i> , N ₃ O ₂	1.10(2)	3.52(2)	31
1		<i>Sp</i> , ^c NO ₄	1.11(2)	3.02(2)	<i>h</i>
2		<i>Sp</i> , NO ₄	1.12(2)	3.00(2)	<i>h</i>
[Fe ₂ (μ-O ₂ CAr ^{Tol}) ₄ (4- ^t BuC ₅ H ₄ N) ₂]		<i>Sp</i> , NO ₄	1.12(2)	3.05(2)	20
[Fe(O ₂ CAr ^{4-^tBuPh}) ₂ (2,2'-bipy) ₂]		<i>Tbp</i> , N ₂ O ₃	1.13(2)	2.91(2)	31
[Fe ₂ (μ-O ₂ CAr ^{Tol}) ₂ (O ₂ CAr ^{Tol}) ₂ (C ₆ H ₅ N) ₂]		<i>Tbp</i> , NO ₄	1.19(2)	2.90(2)	20
[Fe ₂ (μ-O ₂ CAr ^{Tol}) ₂ (O ₂ CAr ^{Tol}) ₂ (Bn ₂ en) ₂]		<i>Tbp</i> , NO ₄	1.19(2)	2.99(2)	35
[Fe ₂ (μ-O ₂ CAr ^{Tol}) ₂ (O ₂ CAr ^{Tol}) ₂ (THF) ₂]		<i>Tbp</i> , O ₅	1.26(2)	2.90(2)	20
[Fe ₄ (μ-OH) ₄ (μ-O ₂ CAr ^{4-^tBuPh}) ₂ (μ-OTf) ₂ (C ₆ H ₅ N) ₄]		<i>Oh</i> , ^d NO ₅	1.27(2)	3.00(2)	<i>j</i>
[Fe ₄ (μ-OH) ₄ (μ-O ₂ CAr ^{4-^tBuPh}) ₂ (μ-OTf) ₂ (4- ^t BuC ₅ H ₄ N) ₄]		<i>Oh</i> , NO ₅	1.26(2)	2.96(2)	<i>j</i>
[Fe ₄ (μ-OH) ₄ (μ-O ₂ CAr ^{4-^tBuPh}) ₂ (μ-OTf) ₂ (3-FC ₆ H ₄ N) ₄]		<i>Oh</i> , NO ₅	1.27(2)	2.90(2)	<i>j</i>
3		<i>Oh</i> , NO ₅	1.29(2)	3.09(2)	<i>h</i>
[Fe ₂ (μ-OH ₂) ₂ (μ-O ₂ CAr ^{Tol}) ₂ (O ₂ CAr ^{Tol}) ₂ (THF) ₂]		<i>Oh</i> , O ₆	1.31(2)	2.86(2)	<i>k</i>
[Fe ₂ (μ-OH ₂) ₂ (μ-O ₂ CAr ^{4F-Ph}) ₂ (O ₂ CAr ^{4F-Ph}) ₃ (THF) ₂ (OH ₂) ₂]		<i>Oh</i> , O ₆	1.35(2)	3.26(2)	18
[Fe ₄ (μ ₃ -OCH ₃) ₄ (O ₂ CAr ^{Tol}) ₄ (HOCH ₃) ₆]	site 1	<i>Oh</i> , O ₆	1.30(2)	3.53(2)	<i>i</i>
	site 2	<i>Tbp</i> , O ₅	1.17(2)	2.35(2)	
MMOH			1.30 ^e	2.87 ^e	<i>l</i>
			1.3 ^{f,g}	2.4–3.1 ^{f,g}	<i>m</i>
RNR-R2			1.26	3.13	<i>n</i>
Δ9D			1.30 ^g	3.04–3.36 ^g	<i>o</i>

^a Tetrahedral. ^b Trigonal bipyramidal. ^c Square pyramidal. ^d Octahedral. ^e *Methylococcus capsulatus* (Bath). ^f *Methylosinus trichosporium* OB3b. ^g Two quadrupole doublets. ^h This work. ⁱ Supporting Information. ^j Lee, D.; Sorace, L.; Caneschi, A.; Lippard, S. J. *Inorg. Chem.* **2001**, *40*, 6774. ^k Kelly, A. E.; Lippard, S. J. Unpublished result. ^l Liu, K. E.; Valentine, A. M.; Wang, D.; Huynh, B. H.; Edmondson, D. E.; Salifoglou, A.; Lippard, S. J. *J. Am. Chem. Soc.* **1995**, *117*, 10174. ^m Pulver, S. C.; Froland, W. A.; Fox, B. G.; Lipscomb, J. D.; Solomon, E. I. *J. Am. Chem. Soc.* **1993**, *115*, 12409. ⁿ Pulver, S. C.; Tong, W. H.; Bollinger, M. J., Jr.; Stubbe, J.; Solomon, E. I. *J. Am. Chem. Soc.* **1995**, *117*, 12664. ^o Fox, B. G.; Shanklin, J.; Somerville, C.; Münck, E.; Proc. Natl. Acad. Sci. U.S.A. **1993**, *90*, 2486.

the following.⁴⁰ The isomer shift is defined by the expression in eq 1, where S and A are two different chemical environments

$$\delta = \text{constant} \times (|\psi_s(0)_S|^2 - |\psi_s(0)_A|^2) \quad (1)$$

with S the sample and A a reference absorber.⁴¹ The expectation value $|\psi_s(0)_S|^2$ describes the *s*-electron density at the iron nucleus. The isomer shift of an iron complex is dictated by two major factors, a direct contribution from 4*s*-electron density and indirect contributions from the 3*d*-electrons that shield the *s*-electrons from penetrating the nucleus.⁴² Since the direct contribution in the series of ferrous complexes in the table is fixed, only the indirect contributions are variable. The shielding can be considered as arising from the nonbonding influence of the 3*d*⁶ electronic configuration of iron(II), attenuated by covalency in which ligands donate an effective total of *x* electrons from their filled orbitals to the metal 3*d*-orbitals and by covalency involving donation of an effective number *y* of 3*d* metal electrons into π^* ligand acceptor orbitals. Thus, the effective number of shielding 3*d*-electrons (*N*_{eff}) can be described by *N*_{eff} = 6 + *x* − *y*. Because the complexes listed in Table 2 have ligand frameworks that are only weakly π acidic, the *y* contribution can be considered to be negligible. The covalency contribution, *x*, is expected to follow the order six- > five- > four-coordination. Larger isomer shifts will therefore occur for complexes having higher *N*_{eff} values, as observed for the compounds listed in Table 2. The complex [Fe₄(μ-OMe)₄(O₂CAr^{Tol})₄(HOMe)₆](HOMe), the synthesis and structure de-

termination (Figure S8) of which are supplied as Supporting Information, contains three octahedral (O₆) and a trigonal bipyramidal (O₅) iron(II) sites and displays two quadrupole doublets in a 3:1 ratio (Figure S9). It is noteworthy that the iron(II) sites with O₆ coordination environments have a larger isomer shift of 1.30(2) mm/s than the iron(II) site with O₅ geometry, 1.17(2) mm/s in this compound.

Superimposed on the effects of coordination geometry is the N/O composition of the coordination environment of iron for the compounds in Table 2. Of particular interest are carboxylate-bridged diiron(II) species with a single N- and a variable number of O-atom donors, which includes compounds **1–3** reported here. These environments represent possibilities for the reduced forms of bacterial multicomponent monooxygenases and related non-heme diiron enzymes.^{3–5} The isomer shift of the diiron(II) sites in reduced sMMOH is reported to be ~1.30 mm s⁻¹,⁶ which is in the range of six coordinate NO₅ iron(II) sites. This comparison suggests that the metal centers in the enzyme may be six-coordinate. The X-ray structural work indicates six ligands in the vicinity of each iron atom, with some of the water molecules interacting only weakly with the diiron(II) center.⁴³ The correlation between coordination number and Mössbauer isomer shift for the NO_x complexes in Table 2 should assist the interpretation of results for other carboxylate-bridged diiron proteins in the literature.

Electronic and Resonance Raman Spectroscopy. The 4-cyanopyridine ligand affords a valuable spectroscopic signature for monitoring the chemistry of its carboxylate-bridged diiron(II) complexes. A similar strategy for investigating the ferrous heme in a cytochrome P450 appeared recently, while this report was in preparation.⁴⁴ The intense colors of **1** and **2**

(40) Dabrowiak, J. C.; Merrell, P. H.; Stone, J. A.; Busch, D. H. *J. Am. Chem. Soc.* **1973**, *95*, 6613–6622.

(41) Drago, R. S. *Physical Methods in Chemistry*; W. B. Saunders Co.: Philadelphia, PA, 1977.

(42) Gibb, T. C. In *Principles of Mössbauer Spectroscopy*; Chapman & Hall: New York, 1976; pp 93–101.

(43) Whittington, D. A.; Lippard, S. J. *J. Am. Chem. Soc.* **2001**, *123*, 827–838.

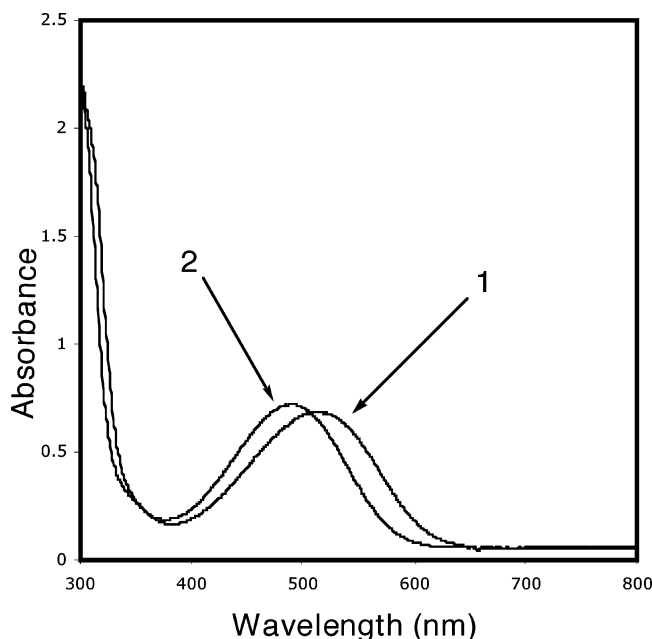
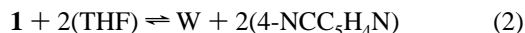


Figure 3. UV-vis spectra of $[\text{Fe}_2(\mu\text{-O}_2\text{CAr}^{\text{Tol}})_4(4\text{-NCC}_5\text{H}_4\text{N})_2]$ (**1**) and $[\text{Fe}_2(\mu\text{-O}_2\text{CAr}^{\text{4F-Ph}})_4(4\text{-NCC}_5\text{H}_4\text{N})_2]$ (**2**) in CH_2Cl_2 .

observed in the solid state are also evident in CH_2Cl_2 solutions of the compounds, with λ_{max} values occurring at 510 nm ($\epsilon = 2200 \text{ cm}^{-1} \text{ M}^{-1}$) and 480 nm ($\epsilon = 2300 \text{ cm}^{-1} \text{ M}^{-1}$), respectively (Figure 3). Considering that the iron(II) sites of **2** are coordinated by carboxylates with more electron-withdrawing groups, the observed difference (blue shift) in the energy of the electronic transition supports a MLCT assignment. To gain more insight into the origin of this unusual electronic transition, the resonance Raman (rR) spectrum of **1** was measured in CH_2Cl_2 solution at ambient temperature with excitation at 514 nm. The result is presented in Figure S10, which displays the spectra of **1** and, for comparison, 4-NCC₅H₄N (literature data). Several strong resonance-enhanced peaks appeared in the 700 cm^{-1} to 1800 cm^{-1} region for **1**. These features are also present in the rR spectrum of the 4-NCC₅H₄N ligand, indicating that the chromophore involves the N-donor ligand. On the basis of the high intensities of the electronic transitions, the blue shift of the more electron-poor iron(II) complex, and the resonance enhanced peaks corresponding to the 4-NCC₅H₄N ligand, the visible bands of **1** and **2** are assigned to an $\text{Fe(II)} \rightarrow 4\text{-NCC}_5\text{H}_4\text{N}$ charge transfer (MLCT) transition.

Equilibria in Coordinating Solvents. No marked thermochromism of **1** occurs in CH_2Cl_2 or toluene solutions of **1**. When coordinating solvents such as THF, acetonitrile, or benzonitrile are employed, however, the visible band of **1** is absent at ambient temperature and grows in as the temperature is lowered (Figure 4, top). The effect is fully reversible. This solvent-dependent thermochromism was further investigated in THF solution, where the complex is more soluble. Addition of 2 equiv of 4-NCC₅H₄N to a THF solution of **1** at ambient temperature restored its red color, indicating the existence of the equilibrium depicted in Scheme 2 and described by eq 2,



where **W** is $[\text{Fe}_2(\mu\text{-O}_2\text{CAr}^{\text{Tol}})_2(\text{O}_2\text{CAr}^{\text{Tol}})_2(\text{THF})_2]$. Fitting the measured absorbance change over a temperature range afforded

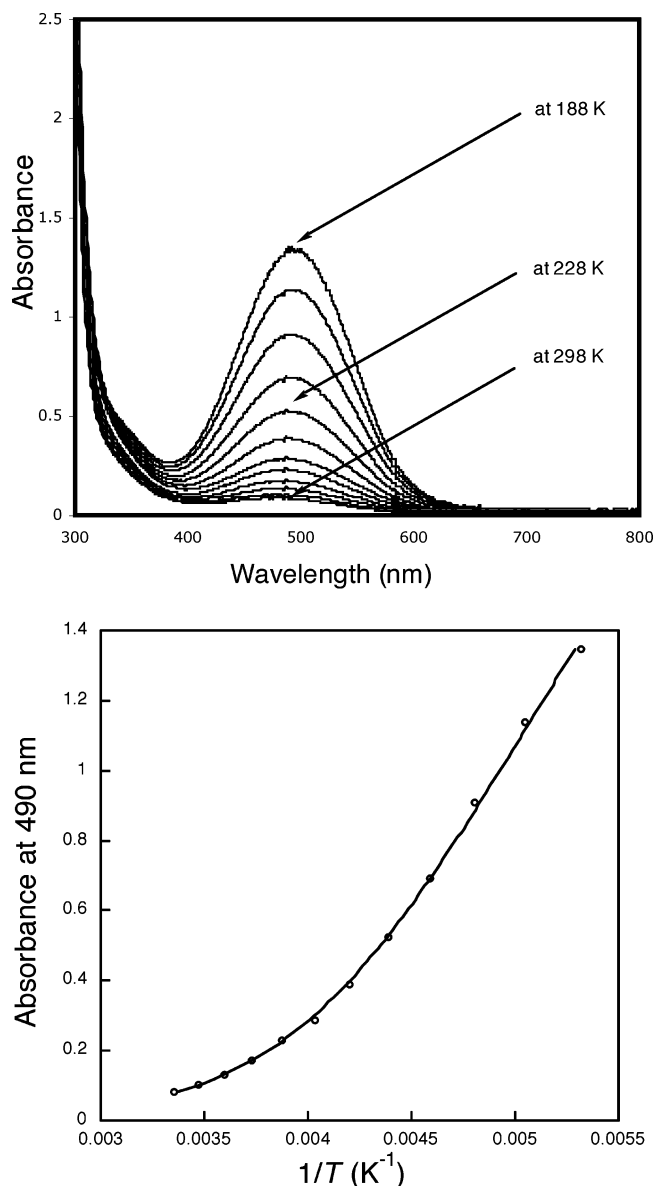
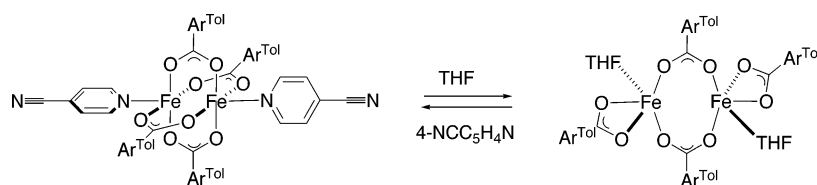


Figure 4. (Top) UV-vis spectra of $[\text{Fe}_2(\mu\text{-O}_2\text{CAr}^{\text{Tol}})_4(4\text{-NCC}_5\text{H}_4\text{N})_2]$ (**1**) in THF, measured at variable temperatures. (Bottom) The absorbance change at 490 nm fit to eq 2; the line represents a least-squares fit to the data points, and the resulting estimated errors for each parameter are shown in parentheses in the text.

a quantitative treatment of the equilibrium. A mathematical equation describing the model of eq 2 is derived in Appendix 1 (Supporting Information), which assumes no change in the extinction coefficient (ϵ) of **1** over the entire temperature range. The resulting thermodynamic parameters are $\Delta H = 19.0$ (6) kJ mol^{-1} , $\Delta S = -16.2$ (16) $\text{J mol}^{-1} \text{ K}^{-1}$, and $\epsilon_{490} = 4650$ (280) $\text{M}^{-1}\text{cm}^{-1}$, with $R = 0.9996$, and the fit is shown in Figure 4 (bottom). The observed thermochromism arises from the small positive enthalpy and negative entropy for the reaction. The electron-withdrawing cyano group of the 4-NCC₅H₄N ligand weakens its donor strength, contributing to the small positive enthalpy. The large excess of the coordinating THF solvent displaces the 4-NCC₅H₄N ligands from **1**. Because of the tendency for coordinating solvents to react with **1**, further studies were carried out in noncoordinating CH_2Cl_2 .

(44) Ost, T. W. B.; Clark, J. P.; Anderson, J. L. R.; Yellowlees, L. J.; Daff, S.; Chapman, S. K. *J. Biol. Chem.* **2004**, 279, 48876–48882.

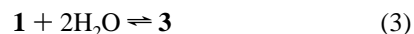
Scheme 2



Water-Dependent Reactions. Recently we reported the observation of water-dependent interconversions involving the compounds $[\text{Fe}_2(\mu\text{-OH}_2)_2(\mu\text{-O}_2\text{CAr}^{\text{Tol}})_2(\text{O}_2\text{CAr}^{\text{Tol}})_2(4\text{-}^t\text{BuC}_5\text{H}_4\text{N})_2]$ ¹⁷ and $[\text{Fe}_2(\text{OH}_2)_2(\mu\text{-O}_2\text{CAr}^{4\text{F-Ph}})_2(\text{O}_2\text{CAr}^{4\text{F-Ph}})_2(\text{THF})_2]$.^{17,18} A quantitative treatment of the putative equilibrium processes was not possible, however, due to the absence of optical spectroscopic bands for following the reactions in solution. When the yellow-red compound **3** is dissolved in

anhydrous CH_2Cl_2 at room temperature, the UV–vis spectrum of the resulting red-pink ($\lambda_{\text{max}} = 510 \text{ nm}$) solution exactly matches that of **1**. Dissolving **1** in CH_2Cl_2 that is saturated with water produces the electronic transition at 460 nm, characteristic of **3** in the solid state. These results indicate that **1** and **3** are related by a water-dependent equilibrium. UV–vis spectra of a CH_2Cl_2 solution of **3** were measured over the temperature range 283 K to 193 K (Figure 5). Upon lowering the temperature from 273 to 203 K, there is a gradual shift of the peak maximum from 510 to 460 nm, with two isosbestic points at 480 and 360 nm. The peak at 510 nm originates from compound **1**, and that at 460 nm is assigned to a water-containing compound **3**. The two isosbestic points suggest that **1** and **3** are the only spectroscopically active species involved in the thermochromic behavior over the temperature range from 273 to 203 K. Below 203 K, however, the absorbance at 460 nm continues to increase and the isosbestic points disappear.

A possible explanation for the observed, reversible thermochromism is the addition of water molecules to **1**, as displayed in Scheme 3. Dissolution of **3** effects the dissociation of water molecules from the diiron site, generating **1**. Binding of water molecules to **1** decreases the absorbance at 510 nm while increasing that at 460 nm, indicating the generation of compound **3**. The disappearance of isosbestic points below 203 K can be explained by both the increased overall molar concentration of all components in solution as temperature decreases and the turbidity arising from the generation of the clathrate $\text{CH}_2\text{Cl}_2 \cdot 34\text{H}_2\text{O}$ at low temperature. The formation of such a clathrate below -40°C in 2–4 mM H_2O in CH_2Cl_2 has been noted previously.⁴⁵ A mathematical equation describing this model (eq 3) is derived in Appendix 2 (Supporting Information).



Fitting the temperature dependence of the observed absorbance change at 510 nm resulted in the thermodynamic and spectral parameters $\Delta H = -95 (11) \text{ kJ mol}^{-1}$, $\Delta S = -253 (47) \text{ J mol}^{-1} \text{ K}^{-1}$, $\epsilon_{510} = 2001 (26) \text{ M}^{-1} \text{ cm}^{-1}$ for **1**, and $\epsilon_{510} = 1090 (8) \text{ M}^{-1} \text{ cm}^{-1}$ for **3** with $R = 0.986$ (Figure 5, bottom). The negative enthalpy results from the energy of bond formation between water and the diiron(II) site, and the negative entropy corresponds to a formally termolecular reaction. Although water binding is not tight at room temperature, it becomes very favorable at low temperature. Recently reported oxygenation studies of diiron(II) complexes in a carboxylate-rich coordination environment described, without explanation, the inhibition of intermediates generated at low temperature by a trace amount of water.⁴⁶ We suggest that the binding of water molecules to

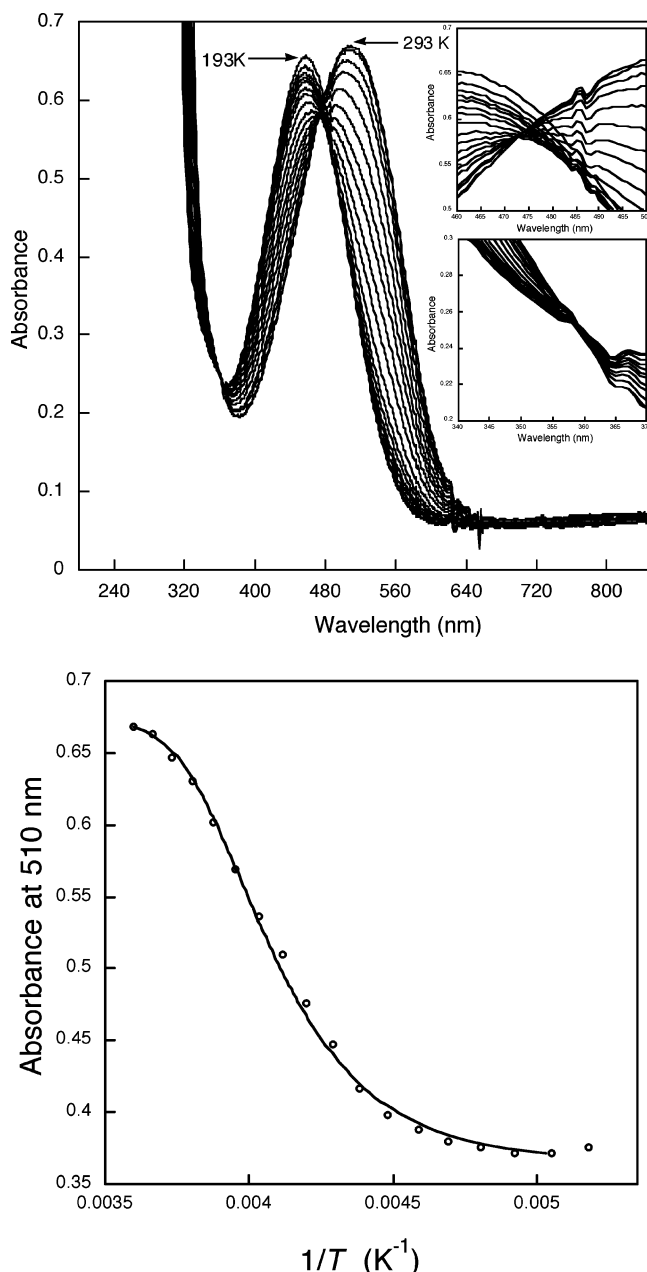
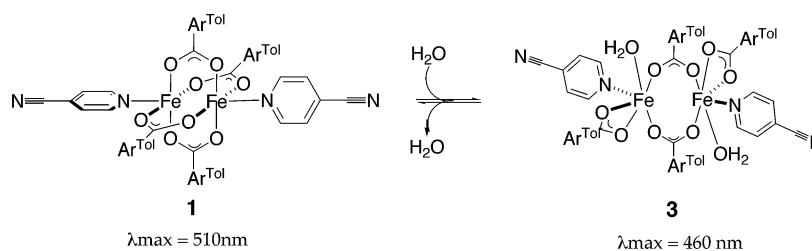


Figure 5. (Top) UV–vis spectra of $[\text{Fe}_2(\mu\text{-O}_2\text{CAr}^{\text{Tol}})_4(4\text{-NCC}_5\text{H}_4\text{N})_2]$ (**3**) in CH_2Cl_2 , measured at variable temperatures. (Bottom) The absorbance change at 510 nm fit to eq 3.

- (45) Kryatov, S. V.; Rybak-Akimova, E. V.; MacMurdo, V. L.; Que, L., Jr. *Inorg. Chem.* **2001**, *40*, 2220–2228, and refs. cited therein.
 (46) Kryatov, S. V.; Chavez, F. A.; Reynolds, A. M.; Rybak-Akimova, E. V.; Que, L., Jr.; Tolman, W. B. *Inorg. Chem.* **2004**, *43*, 2141–2150, and refs. cited therein.

Scheme 3



their carboxylate-rich diiron(II) complexes at low temperature may be the cause of this behavior.

The properties observed for the present complexes have not yet been encountered for diiron(II) units having nitrogen-rich environments, suggesting perhaps that carboxylate-rich coordination spheres might be especially amenable to supporting diverse geometries depending on the amount of water available. Our findings thus suggest the possible occurrence of related water-dependent equilibria in enzymes having several glutamate or aspartate ligands bound to their diiron centers, and variable numbers of water molecules are indeed encountered at the active sites of sMMOH,⁴³ RNR-R2,⁴⁷ $\Delta^9\text{D}$,⁸ and ToMOH.¹⁰ In reduced sMMOH, for example, there are two water molecules, compared with no water molecules at all at the diiron(II) core of $\Delta^9\text{D}$. During catalysis the accessible amount water at the non-heme diiron(II) sites may differ even more and function to allow a shared structural motif to achieve its diverse roles.

Effect of Water on the Oxygenation Rate of Compound 1

1. The influence of water on the oxygenation chemistry of carboxylate-rich diiron(II) complexes is of interest because the active sites in reduced sMMOH contain two water molecules in the first and second coordination spheres. Such water may modulate the oxygenation reactions of the diiron(II) centers in the enzyme. The reaction of compound **1** with dioxygen instantaneously produces a light yellow-green solution. The kinetics of this process were followed by stopped-flow spectroscopy, monitoring the charge-transfer band, a broad feature centered at 510 nm for **1** (Figure 6). When examined in the presence of excess dioxygen, the decay of compound **1** follows a pseudo first-order rate law. Rate constants (Table 3) were

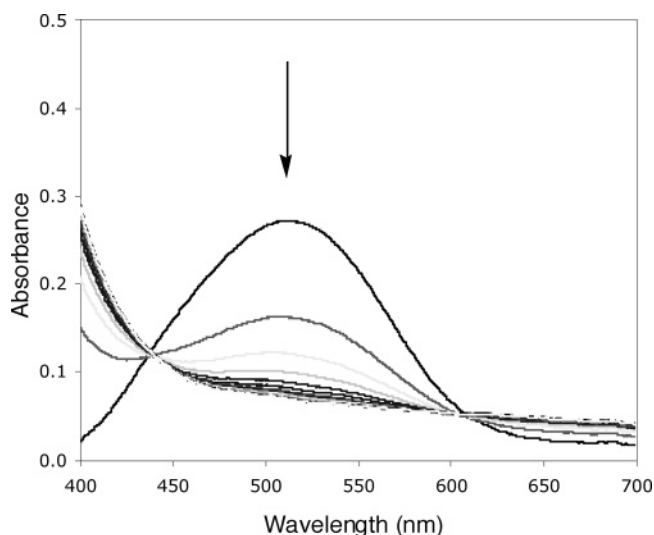
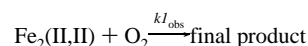


Figure 6. Spectral changes occurring during oxygenation of **1** (1.74×10^{-4} M) without water in CH_2Cl_2 at 273 K over 20 s.

Table 3. Rate Constants ($k_{1\text{obs}}^a$) for Oxygenation of **1** in CH_2Cl_2

temperature (K)	$k_{1\text{obs}}$
293	1.4(3)
283	0.71(6)
273	0.40(2)
263	0.20(1)
253	0.10(1)
243	0.045(5)

^a $k_{1\text{obs}}$ is defined by the following reaction:



derived from time-dependent absorbance changes by using a nonlinear least-squares fitting procedure based on eq 4, where

$$A_t = A_\infty - (A_\infty - A_0)\exp(-k_{\text{obs}}t) \quad (4)$$

A_∞ and A_0 are the optical absorbances at infinite and zero times, respectively. The fast oxygenation of **1** in solution contrasts with its observed inertness to O_2 in the solid state, indicating that the reactive species in solution may not have a quadruply bridged diiron(II) structure. An equilibrium between doubly and quadruply bridged isomers of **1** in the solution state is likely to occur, with concomitant carboxylate shifts. Such an equilibrium has been proposed and is generally accepted for the analogous complex, $[\text{Fe}_2(\mu\text{-O}_2\text{CAR}^{\text{Tol}})_4(4\text{'BuC}_5\text{H}_4\text{N})_2]$.³⁶ One of these isomers, probably a doubly bridged complex, would react with dioxygen.

Competition between dioxygen and water for **1** was investigated between 193 and 293 K by using stopped-flow kinetics. To obtain pseudo-first-order conditions, the concentrations of **1**, water, and dioxygen were maintained at 0.19, 1.00, and 2.9 mM, respectively. The reaction proceeds through the extremely fast generation of a species that absorbs at 460 nm and subsequently decays (Figure 7). The first steps were only detectable at temperatures below 223 K and went to completion within 1 s. The time-dependent absorbance changes follow a pseudo first-order rate law and the fit results are listed in Table 4. The second step proceeds considerably more slowly than the first. The decay at 460 nm also follows a pseudo first-order rate law, and rate constants were determined by a linear squares fit to eq 4. The kinetic behavior can be rationalized by the following scenario (Scheme 4). The species with an absorption maximum at 460 nm, the formation of which is correlated with the decrease of the band at 510 nm, is assigned as the water-containing compound **3**, generated by aquation of **1** (see above), and the decay of this peak occurs through oxygenation. This analysis provides two important insights. First, aquation of **1** is at least 1000 times faster than oxygenation of **1**. The rate constant for aquation ($k_{2\text{obs}}$) of **1** at 223 K is $63.5(8) \text{ s}^{-1}$, whereas

(47) Nordlund, P.; Eklund, H. *J. Mol. Biol.* **1993**, 232, 123–164.

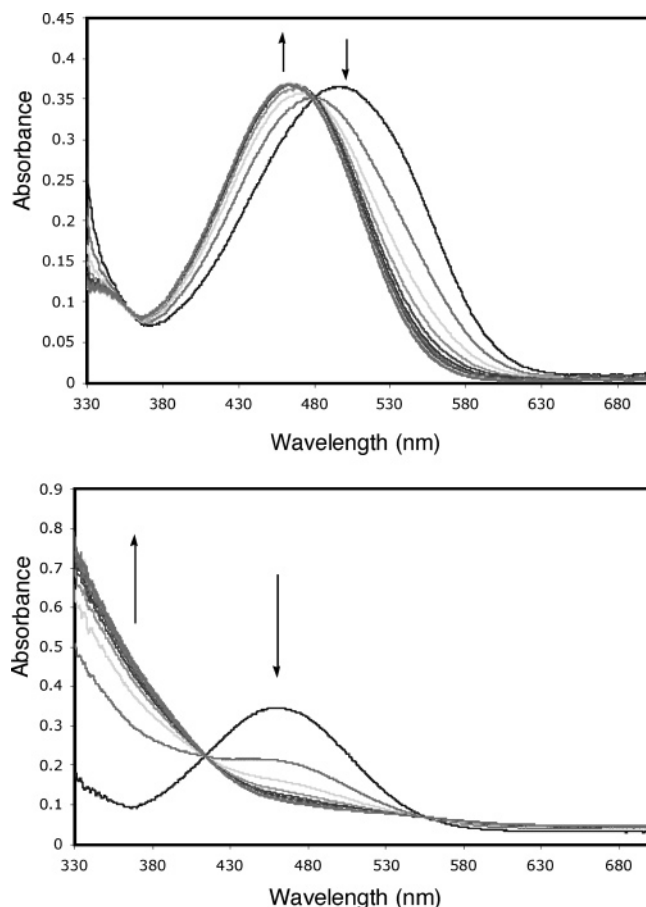
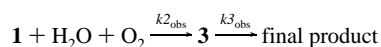


Figure 7. (Top) Spectral changes that occur during the reaction of **1** (1.60×10^{-4} M) with dioxygen and water in CH_2Cl_2 at 213 K over 1 s. (Bottom) Spectral changes that occur during oxygenation of **1** (1.60×10^{-4} M) with dioxygen and water in CH_2Cl_2 at 253 K over 10 s.

Table 4. Rate Constants $k_{2\text{obs}}$ and $k_{3\text{obs}}$ for Oxygenation of **1** in CH_2Cl_2 with Water

temperature (K)	$k_{2\text{obs}}$ (s^{-1}) ^a	temperature (K)	$k_{3\text{obs}}$ (s^{-1}) ^a
223	62.8(5)	293	14.6(7)
218	43.0(24)	283	9.1(10)
213	23.7(17)	273	5.5(5)
208	11.1(8)	263	2.7(2)
203	5.1(2)	253	1.21(17)
198	2.5(1)	243	0.39(12)
		233	0.12(1)

^a $k_{2\text{obs}}$ and $k_{3\text{obs}}$ are defined by following the reaction:



that for oxygenation ($k_{1\text{obs}}$) at 243 K is $0.045(5) \text{ s}^{-1}$. This dramatic difference in rate constants may originate from the small but obvious size difference between water and dioxygen and the hydrogen bond donating ability of the former. Second, the water-containing compound **3** reacts with dioxygen ca. 10-fold faster than does **1**. We suggest that the lability of the water ligands in **3** affords an open coordination site for dioxygen binding (Scheme 4), an event that may facilitate Fe–O₂ bond formation, which is presumably the rate-determining step for oxidation.

Isolation and Structural Characterization of Iron(III) Complexes $[\text{Fe}_2(\mu\text{-OH})_2(\mu\text{-O}_2\text{Car}^{\text{Tot}})_2(\text{O}_2\text{Car}^{\text{Tot}})_2\text{-}(4\text{-NCC}_5\text{H}_4\text{N})_2] \cdot 2(\text{HO}_2\text{Car}^{\text{Tot}})$ (**6**) and $[\text{Fe}_6(\mu\text{-O})_2(\mu\text{-OH})_4(\mu\text{-O}_2\text{Car}^{\text{Tot}})_6(4\text{-NCC}_5\text{H}_4\text{N})_4(\text{Cl})_2]$ (**7**). Vapor diffusion of pentane

Scheme 4

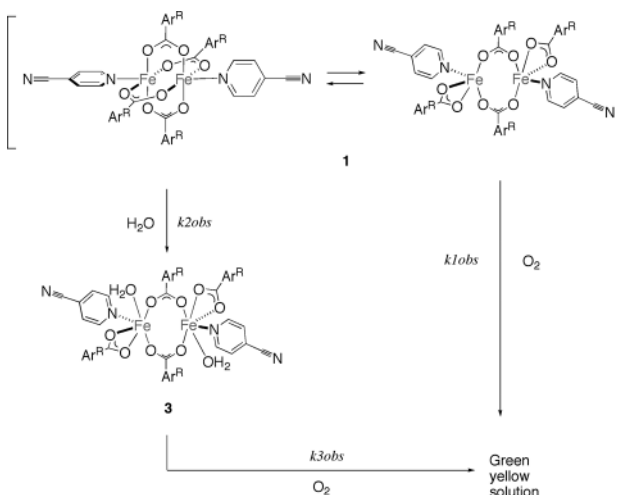


Table 5. Selected Interatomic Distances (Å) and Angles (deg) for **6**^a

Fe1...Fe2	2.8323(10)	Fe2–O6	2.033(3)
Fe1–O1	1.950(3)	Fe2–N3	2.127(4)
Fe1–O2	1.978(3)	O8...O1	2.888(5)
Fe1–O3	2.045(3)	O8...O11	2.639(5)
Fe1–O5	2.076(3)	O10...O13	2.636(5)
Fe1–O7	1.955(3)	O10...O2	2.814(6)
Fe1–N1	2.132(4)	Fe1–O1–Fe2	43.50(10)
Fe2–O1	1.999(3)	Fe1–O2–Fe2	43.33(10)
Fe2–O2	1.945(3)	O1–Fe1–O2	88.19(14)
Fe2–O4	2.053(3)	O1–Fe2–O1	87.75(14)

^a Numbers in parentheses are estimated standard deviations of the last significant figure. Atoms are labeled as indicated in Figure 8.

Table 6. Selected Interatomic Distances (Å) and Angles (deg) for **7**^a

Fe1...Fe2	3.064(4)	Fe2–O10	2.059(7)
Fe2...Fe3	2.960(3)	Fe2–O6	2.085(7)
Fe1...O1	1.881(7)	Fe2–O12	2.019(8)
Fe1–O2	2.029(7)	Fe3–O7	2.063(7)
Fe1–O3	2.004(7)	Fe3–N2	2.181(9)
Fe1–O4	2.042(8)	Fe3–Cl(1)	2.311(3)
Fe1–O11	2.103(7)	Fe1–O3–Fe2	99.9(3)
Fe2–O3	1.999(7)	Fe1–O4–Fe2	97.5(4)
Fe2–O4	2.034(9)	Fe2–O12–Fe3	95.7(3)

^a Numbers in parentheses are estimated standard deviations of the last significant figure. Atoms are labeled as indicated in Figure 9.

into the light greenish-yellow CH_2Cl_2 solution generated upon oxygenation of **1** affords crystals, an inseparable mixture of the quadruply bridged diiron(III) complex **6** and the hexairon(III) species **7**. The structure of **6** is depicted in Figure 8, and selected interatomic distances and angles are listed in Table 5. Two distorted octahedral iron(III) atoms are bridged by two hydroxide and two carboxylate ligands. The Fe...Fe distance of 2.8323(10) Å is in the ~ 2.85 Å range typical for previously reported quadruply bridged $\{\text{Fe}_2(\mu\text{-OH})_2(\mu\text{-O}_2\text{CR})_2\}^{2+}$ cores.³⁶ Two intramolecular hydrogen bonding interactions occur between the terminal, metal-bound carboxylates and the bridging hydroxo groups, with O–H...O distances of 2.818(6) and 2.888(5) Å. In addition, two carboxylic acids ($\text{HO}_2\text{Car}^{\text{Tot}}$) are located in proximity to the terminal carboxylates in the crystal lattice, generating hydrogen-bonding interactions.

The hexairon(III) species **7** was isolated with compound **6**. Its structure is best described by the diagrams in Figure 9, and a list of selected interatomic distances and angles is included

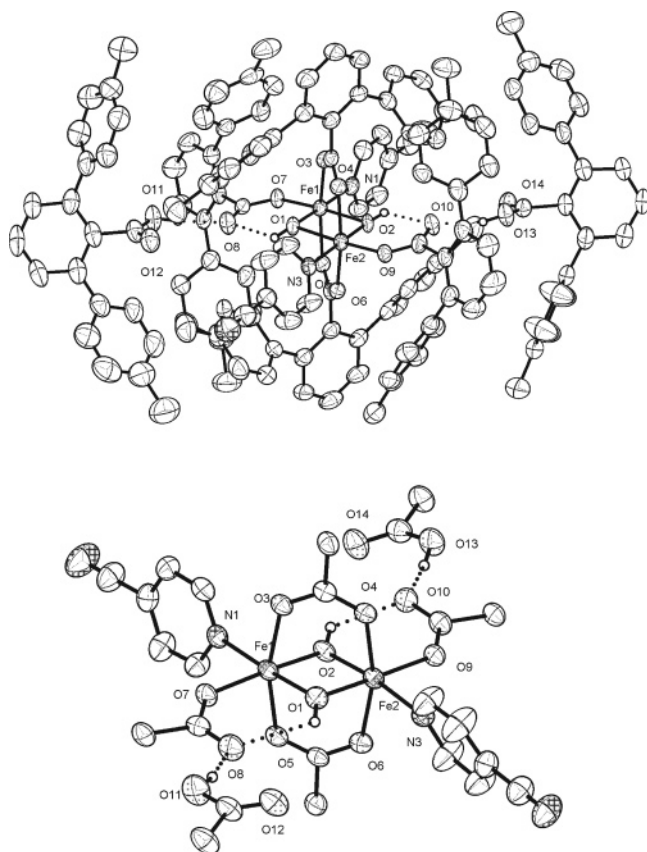


Figure 8. Top: ORTEP diagram of $[\text{Fe}_2(\mu\text{-OH})_2(\mu\text{-O}_2\text{CAr}^{\text{Tol}})_2(\text{O}_2\text{CAr}^{\text{Tol}})_2\text{-(4-NCC}_5\text{H}_4\text{N)}_2(\text{OH}_2)_2]\cdot 2(\text{HO}_2\text{CAr}^{\text{Tol}})_2$ (**6**) showing 50% probability thermal ellipsoids for all non-hydrogen atoms. Bottom: View of the structure with the aromatic rings of $\text{Ar}^{\text{Tol}}\text{CO}_2^-$ ligands omitted for clarity.

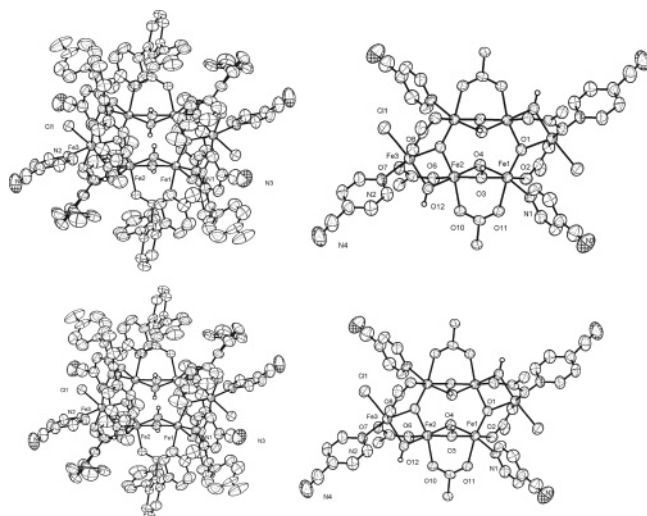


Figure 9. Top left: ORTEP diagram of **7** showing 50% probability thermal ellipsoids for all non-hydrogen atoms. Top Right: The aromatic rings of $\text{Ar}^{\text{Tol}}\text{CO}_2^-$ ligands are omitted for clarity. Bottom: View of the structure with the aromatic rings of $\text{Ar}^{\text{Tol}}\text{CO}_2^-$ and $4\text{-NCC}_5\text{H}_4\text{N}$ omitted for clarity.

in Table 6. The structure of **7**, which has an inversion center, combines two $(\mu_3\text{-oxo})\text{triiron(III)}$ units through four OH^- and two $\text{O}_2\text{CAr}^{\text{Tol}}$ bridging groups. Four octahedral and two distorted trigonal bipyramidal iron(III) sites result. It is noteworthy that the structure of **7** also contains two Cl^- ligands coordinated to each of the octahedral iron(III) sites. When the

experiment was performed in the absence of light, the same mixture of **6** and **7** resulted, indicating that a photochemical reaction is not involved in generating the Cl^- anion.

Mechanistic Considerations. Based on the spectroscopic, structural, and kinetic data obtained, a mechanism is proposed to account for the observed chemical conversions (Scheme 4). An equilibrium between the doubly and quadruply bridged isomers of **1** in the solution state can occur through carboxylate shifts. One of these isomers, most likely the doubly bridged complex, reacts with dioxygen faster than the other, quadruply bridged one. This explanation accounts for the marked difference in the oxygenation of solid versus solution samples of **1**. In the competition between water and dioxygen, aquation occurs first and the resulting aqua complex then reacts with dioxygen. The faster reaction rate of the aquated species compared to **1** is ascribed to the favorable formation of an available coordination site generated by rapid, reversible dissociation of water. Oxidation of the solvent, CH_2Cl_2 , generates Cl^- anions, which coordinate to the iron(III) site, leading to reorganization of the diiron species to hexanuclear **7**. The dissociated carboxylic acid interacts with a diiron(III) unit through hydrogen-bonding in compound **6**.

Summary

High-spin 4-cyanopyridine diiron(II) carboxylate complexes with distinctive charge transfer transitions in the visible region have been prepared and used to investigate quantitatively their water-dependent reaction chemistry. Utilizing optical spectroscopy, we were able both to determine the thermodynamic constants for the water-dependent equilibrium and to monitor kinetically the effects of water on the oxygenation of the diiron(II) complex **1**. We propose that a rapidly exchanging water molecule in **3** will generate an open coordination site, accelerating the oxygenation step compared to the reaction under anhydrous conditions. The final products of oxidation are the dinuclear complex **6** and a Cl^- -containing iron(III) oligomer. Finally, by comparison of the new diiron(II) complexes with related ones in the literature, we established a correlation between Mössbauer effect isomer shifts and coordination number for high-spin iron(II) complexes in an oxygen-rich coordination environment. The trend was rationalized on the basis of the s-electron density at the iron nucleus across the series.

Acknowledgment. This work was supported by Grant GM32134 from the National Institute of General Medical Sciences. NMR spectra were measured by using a Bruker 400 spectrometer purchased with assistance from the NIH under Grant 1S10RR13886-01. We thank Ms. Elizabeth Nolan for assistance in measuring Raman spectra, which were obtained in the Harrison Spectroscopy Laboratory at MIT, funded in part by NSF and NIH.

Supporting Information Available: Experimental details for the synthesis and characterization of $[\text{Fe}_4(\mu\text{-OMe})_4(\text{O}_2\text{CAr}^{\text{Tol}})_4\text{-(HOMe)}_6](\text{HOMe})$, including X-ray crystallographic information (Tables S1, S4; Figure S8); Table S1, also summarizing X-ray crystallographic information for **1–7**; Tables S2 and S3 providing geometric parameters for **1–4**; Figures S1–S5 showing ORTEP diagrams including atom labels for **1–5**; Figures S6, S7, and S9, illustrating Mössbauer data and fits for

1–3, 5, $[\text{Fe}_4(\mu\text{-OMe})_4(\text{O}_2\text{CAr}^{\text{Tol}})_4(\text{HOMe})_6](\text{HOMe})$, and $[\text{Fe}(\text{O}_2\text{CAr}^{\text{4F-Ph}})_2(\text{Hdmpz})_2]$; and resonance Raman spectra of **1** and 4-NCC₅H₄N at 23 °C (Figure S10). Derivations of eqs 2 and 3 are also supplied as Appendices 1 and 2, respectively.

This material is available free of charge via the Internet at <http://pubs.acs.org>.

JA0512531